UC Santa Barbara
UC Santa Barbara Previously Published Works

Title

The use of hot-pressing to reduce grain boundary resistance in Nasicon of nominal composition Na3Zr2Si2PO12

Permalink

Authors

Kimura, Makoto
Tseng, Kang-Ting
Wolfenstine, Jeff
et al.

Publication Date
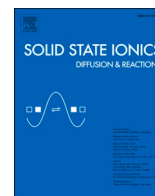
DOI

Peer reviewed

The use of hot-pressing to reduce grain boundary resistance in Nasicon of nominal composition Na$_3$Zr$_2$Si$_2$PO$_{12}$

Makoto Kimura [a], Kang-Ting Tseng [a], Jeff Wolfenstine [b], Jeff Sakamoto [c,*]

[a] Materials Science and Engineering Department, University of Michigan, Ann Arbor, MI 48109, United States of America
[b] Mechano-chemical Understanding of Solid Ion Conductors (MUSIC), A Department of Energy, Energy Frontier Research Center, Seattle, WA 98115, United States of America
[c] Materials Department & Department of Mechanical Engineering, University of California, Santa Barbara, Santa Barbara, CA 93106–5160, United States of America

ABSTRACT

Nasicon powders of nominal composition Na$_3$Zr$_2$Si$_2$PO$_{12}$ were hot-pressed at temperatures of 1150, 1200 and 1250 °C. At room temperature a total conductivity of 4.2 × 10^{-3} S/cm was exhibited, approaching bulk conductivity values (5–6 × 10^{-3} S/cm). The results of impedance spectroscopy combined with microstructural examination and analytical electron microscopy suggested that the high conductivity is a result of the applied stress during hot-pressing. It is believed that the applied stress at high temperatures causes expulsion of molten glass, thereby reducing the thickness of the high resistance glassy phase along Nasicon grain boundaries. This leads to reduced grain boundary resistance and hence, a higher total conductivity than that observed for sintered samples, where no applied stress is present.

1. Introduction

Recently, Na batteries have become of high interest for use in many potential energy storage systems. These include: 1) room temperature all solid batteries with a Na metal anode [1], 2) Na seawater batteries, using seawater as the active cathode [2], 3) low-temperature (<200 °C) molten Na anode batteries [3] and 4) Na-ion aqueous redox flow cell batteries [4]. For these batteries, the major requirements for the Na-ion conducting solid electrolyte are [5]: 1] high Na-ion conductivity, 2] low electronic conductivity and 3] chemical/electrochemical stability with anodes/cathodes.

A possible Na-ion conducting solid electrolyte that is under consideration for the above advanced rechargeable Na batteries is Nasicon (Na Super Ionic Conductor), with the chemical formula Na$_{1+x}$Zr$_2$Si$_x$P$_{3-x}$O$_{12}$, 0 < x < 3 [6]. The most widely used Nasicon at present has the following composition: Na$_3$Zr$_2$Si$_2$PO$_{12}$. In order to obtain dense Na$_3$Zr$_2$Si$_2$PO$_{12}$ solid electrolytes with high ionic conductivity, powders are typically sintered at temperatures between 1100 and 1300 °C [6–22] (sintering refers to densification using only heat with no pressure). It is observed that as the sintering temperature increases the conductivity increases because of an increase in relative density and grain size. However, at higher sintering temperatures (>1200 °C) decomposition of Na$_3$Zr$_2$Si$_2$PO$_{12}$ and/or volatilization of Na and P occurs leading to the

formation of a high resistance glassy phase and ZrO$_2$ particles residing along grain boundaries [8,9,11,14–16,18,22,24]. It has been suggested in the literature that this results in an increase in grain boundary resistance limiting total conductivity to <1 × 10^{-3} S/cm [11,15,17,18,20,22–26]. One possible solution to decrease grain boundary resistance is to reduce the amount of the glassy phase along Na$_3$Zr$_2$Si$_2$PO$_{12}$ grain boundaries by applying a compressive stress during sintering (i.e., hot-pressing). It is known from creep studies on ceramic materials containing a glass phase along grain boundaries that after testing the glass phase was observed on the outside surfaces of the crept samples, whereas none was observed on samples that were only heated with no applied stress [27–29]. It is believed that at high temperatures where the glass can flow, the application of an applied stress causes the glass to flow from the grain boundaries in the interior to outside surfaces, whereas in contrast no glass flow occurs with heat only, leading to the reduction/removal of the glassy grain boundary phase (Fig. 1), which in the case of Na$_3$Zr$_2$Si$_2$PO$_{12}$ should decrease grain boundary resistance and hence, increase total conductivity.

It is the purpose of this paper to show that hot-pressing of Na$_3$Zr$_2$Si$_2$PO$_{12}$ leads to a decrease in grain boundary resistance by reducing the thickness of the glassy phase along grain boundaries, yielding higher conductivities than those obtained using conventional sintering, with total conductivity values approaching bulk conductivity values.

---

* Corresponding author.
  E-mail address: sakamoto@ucsb.edu (J. Sakamoto).

Pressureless   Hot Press
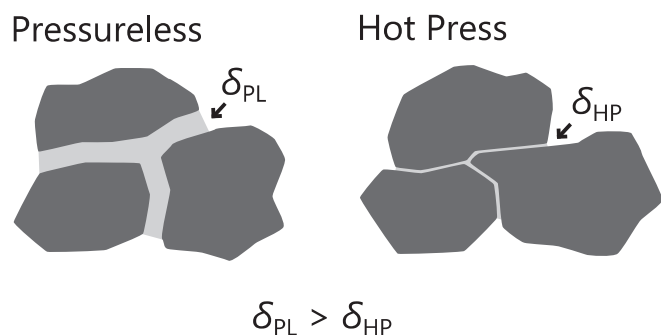
$\delta_{PL} > \delta_{HP}$

Fig. 1. The effect of stress during hot-pressing on reducing the thickness of the glassy grain boundary phase compared to conventional sintering, where no applied stress is used.

2. Experimental

Nasicon powder of nominal composition $Na_3Zr_2Si_2PO_{12}$ was obtained from MSE Supplies LLC (Tucson, AZ). The powder was heat-treated at 400 °C for 24 h under air prior to use. The heat-treated powder was pressed into billets, placed in a graphite die, and consolidated using rapid induction hot pressing (RIHP) at 1150, 1200, or 1250 °C at 30 MPa under flowing argon gas for 40 min. The hot-pressed billets were cut into ~1 mm thick pellets using a diamond saw. Both surfaces of the disk-shaped pellets were polished using 220 to 1200-grit abrasive papers, followed by 15 to 0.1 μm diamond polishing. The thickness of the polished pellets was ~0.5 mm. In addition, a cold-pressed disk of the heat-treated powder was sintered at 1250 °C for 40 min.

The phase purity of the as-received powder, hot-pressed and sintered samples was characterized using X-ray diffraction (XRD) with Cu Kα radiation (Miniflex 600, Rigaku). XRD data was collected between 5 and 120° with a step size of 0.02°. The amount of the crystalline phases was determined by Rietveld refinement using the RIETAN-FP program [30]. The microstructure of the hot-pressed and sintered samples was observed by scanning electron microscopy (SEM). Secondary electron (SE) images of fracture surfaces were obtained using a scanning electron microscope (MIRA3 FEG-SEM, TESCAN). Backscattered electron (BSE) images on polished surfaces were obtained using another scanning electron microscope (TM3030, Hitachi). The amount of the phases/porosity and their location was determined from BSE images using image processing software (ImageJ). The grain size was determined by analyzing SE fracture surface images [31]. A circle was drawn on the images. The total number of grains, n_{tot}, was given as follows [31]:

$$n_{tot} = n_{inside} + \frac{n_{on\ line}}{2} \tag{1}$$

where n_{inside} was the number of grains entirely within the circle and $n_{on\ line}$ was the number of grains on the circumference of the circle. The mean grain area, $\overline{a}_{grain}$, and the mean grain size, $\overline{d}_{grain}$, were calculated from the following equations:

$$\overline{a}_{grain} = \frac{a_{circle}}{n_{tot}} \tag{2}$$

$$\overline{d}_{grain} = \overline{a}_{grain}^{\frac{1}{2}} \tag{3}$$

where a_{circle} was the circle area. Eq. (3) assumes square-shaped grains.

The ionic conductivity of the hot-pressed and sintered samples was measured by electrochemical impedance spectroscopy (EIS) at room temperature and low temperatures for the hot-pressed samples (−78 to −35 °C) in the frequency range of 1 Hz to 7 MHz with a perturbation amplitude of 10 to 500 mV, depending on the ionic resistance of the sample. A BioLogic VMP300 and EC-Lab V11.33 software were used to conduct the EIS measurements. EIS was performed on 3 to 5 pellets at
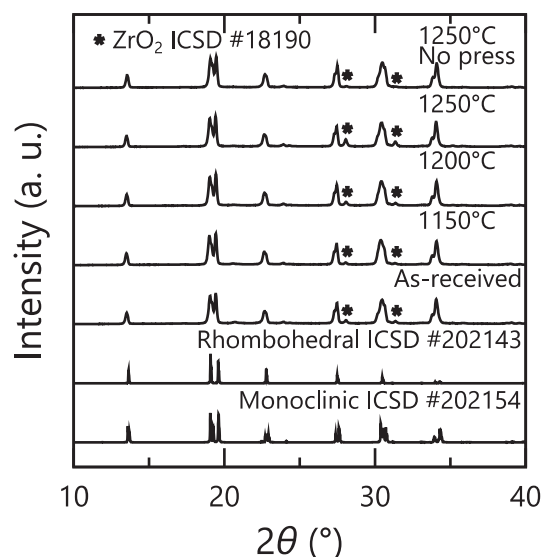

Fig. 2. Room temperature X-ray diffraction patterns of the as-received, sintered and hot-pressed $Na_3Zr_2Si_2PO_{12}$.

Table 1
Rietveld refinement of as-received, sintered and hot-pressed $Na_3Zr_2Si_2PO_{12}$.

Temp. (°C)	Pressure (MPa)	NASICON (wt%)		ZrO_2 (wt%)	R_{wp} (%)
		Monoclinic	Rhombohedral		
(As-received)		81.4 ± 2.2	15.1 ± 1.0	3.5 ± 0.1	9.0
1150	30	84.5 ± 2.2	13.4 ± 1.0	2.1 ± 0.1	9.0
1200	30	81.4 ± 2.0	14.8 ± 0.9	3.8 ± 0.1	8.8
1250	30	79.5 ± 1.9	13.2 ± 0.9	7.3 ± 0.2	8.4
1250	0	83.9 ± 1.9	14.7 ± 0.9	1.4 ± 0.1	8.7

each temperature. Gold electrodes were sputter-coated on both surfaces of the polished pellets. Low temperatures were achieved using a dry-ice bath with ethanol and ethylene glycol solvent mixtures [32].

The elemental composition of the phases in the hot-pressed samples was analyzed using wavelength dispersive X-ray spectrometry (WDS) on a Cameca SX100 electron microprobe. WDS is used rather than energy dispersive X-ray spectrometry (EDS) because of the higher spectral resolution of WDS (~ 10 eV) compared to EDS (~ 130 eV) [33]. This is critical for the case of $Na_3Zr_2Si_2PO_{12}$ because of the overlap of the ZrLα and PKα X-ray lines, as shown in the EDS spectrum (Fig. S1). In contrast, the WDS spectrum (Fig. S1) shows a clear separation of these lines. Thus, using EDS as was done by most of the previous studies [11,13,24] to determine the elemental composition of the phases in $Na_3Zr_2Si_2PO_{12}$ can lead to inaccurate results.

3. Results and discussion

3.1. X-ray diffraction

To determine the crystalline phases and their relative amounts present, X-ray diffraction (Fig. 2) and Rietveld refinement (Fig. S2 and Table 1) was conducted on the as-received powders, the sintered sample and the 1150, 1200 and 1250 °C hot-pressed $Na_3Zr_2Si_2PO_{12}$ samples. From Fig. 2 it is observed that the majority crystalline phase present is Nasicon with a small amount of second phase ZrO_2. From Table 1 several important points are noted. Firstly, the Nasicon phase is mainly monoclinic with a small amount of rhombohedral (about 13–15 wt%). Secondly, the amount of ZrO_2 increases with increasing hot-pressing temperature. This is in agreement with sintering studies, which reveal that as the sintering temperature increases the amount of ZrO_2 increases [10–12,15,18]. Thirdly, there is a slight decrease in the amount of ZrO_2
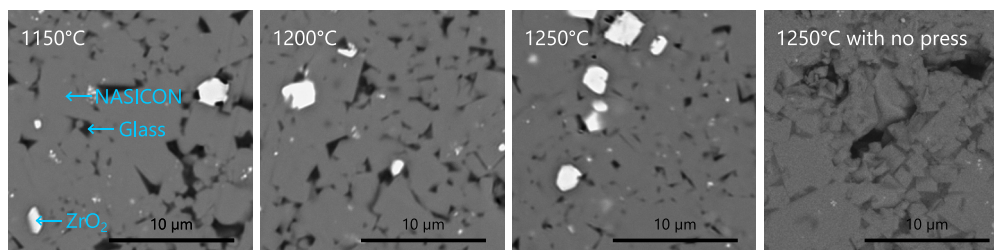
Fig. 3. Backscattered electron images of hot-pressed and sintered $Na_3Zr_2Si_2PO_{12}$. Regions representative of $Na_3Zr_2Si_2PO_{12}$ grains (light grey), glassy phase (dark grey), and ZrO_2 (white) are indicated in the images.

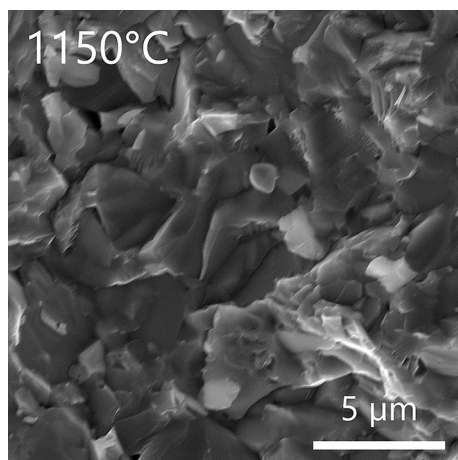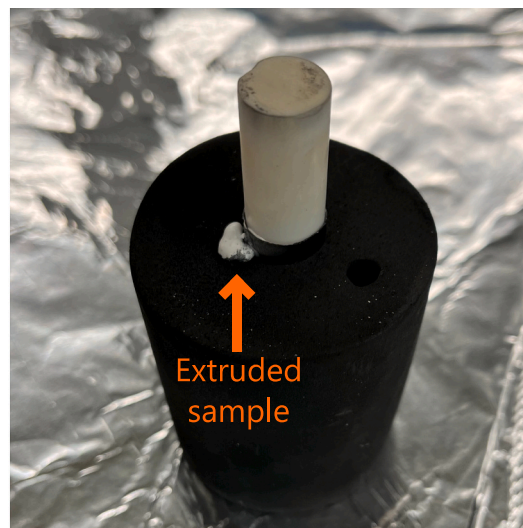**Fig. 4.** Fracture surface of the 1250 °C hot-pressed $Na_3Zr_2Si_2PO_{12}$.

Table 2
Area percentage of the different phases and grain sizes of sintered and hot-pressed $Na_3Zr_2Si_2PO_{12}$.

Temp. (°C)	Pressure (MPa)	Grain size (µm)	NASICON (area%)	Glassy (area%)	ZrO_2 (area%)	Pores (area%)
1150	30	1.37 ± 0.21	90.4 ± 0.2	7.5 ± 0.2	2.04 ± 0.08	< 0.5
1200	30	1.26 ± 0.11	90.4 ± 0.4	6.8 ± 0.6	2.8 ± 0.2	< 0.5
1250	30	1.37 ± 0.12	89.7 ± 1.2	4.9 ± 0.8	5.5 ± 0.4	< 0.5
1250	0	–	64.4 ± 2.3	10.3 ± 2.3	0.6 ± 0.4	24.8 ± 3.1

after hot-pressing at 1150 °C compared to the as-received powders, this is most likely as a result of the reaction of unreacted ZrO_2 in the as-received powders during hot-pressing to form Nasicon.

3.2. Microstructure

Scanning electron microscopy was conducted to examine the microstructure of the hot-pressed and sintered materials. Backscattered electron images of the 1150, 1200 and 1250 °C hot-pressed materials are shown in Fig. 3. All samples show three distinct regions, light grey, dark grey, and white, which has been described in the literature [11,16,24] to represent crystalline Nasicon, glassy phase, and ZrO_2, respectively. The glassy phase is located intergranular along Nasicon grain boundaries. The ZrO_2 particles are located both within Nasicon grains and along Nasicon grain boundaries. Fig. 4 is a fracture surface of the 1250 °C hot-pressed material. From Fig. 4 it is observed that the fracture is primarily transgranular. The relative amount of the phases, porosity and grain size determined from BSE and fracture surface images are given in Table 2.

Fig. 5. Die after hot-pressing at 1250 °C showing an extruded material.

From Table 2 several important points are noted. Firstly, hot-pressing yields high relative density materials, and the porosity is <0.5 area %, compared to about 25% for the sintered material. Secondly, the grain size of the three hot-pressed materials is nearly the same, about 1.2–1.4 µm. Thirdly, the amount of ZrO_2 increases with increasing hot-pressing temperature, in agreement with the X-ray diffraction results (Table 1). Fourthly, as the hot-pressing temperature increases the amount of the glassy phase decreases. In summary the X-ray diffraction and microstructure results reveal that the main differences between the 1150, 1200 and 1250 °C hot-pressed $Na_3Zr_2Si_2PO_{12}$ materials are as follows: 1] the amount of ZrO_2, which increases with increasing hot-pressing temperature and 2] the amount of the glassy phase, which decreases with increasing hot-pressing temperature.

3.3. Chemical analysis

Fig. 5 is a picture of the hot-pressing die after hot-pressing at 1250 °C. From Fig. 5 it is observed that a noticeable volume of material was expelled from the die and accumulated at the base of the alumina anvil. This extruded material was only observed when hot-pressing at 1250 °C. It was surmised that the expelled material was molten at one point, flowed, and accumulated at the base of the anvil on the top side of the hot-pressing die. X-ray diffraction of the extruded material indicates that in addition to monoclinic and rhombohedral Nasicon and crystalline ZrO_2, crystalline Na_3PO_4 was also observed (Fig. S3). However, SEM image analysis revealed that the glassy phase is the majority phase in the extruded material.

The composition of the extruded glassy and Nasicon phases for the 1150, 1200 and 1250 °C hot-pressed $Na_3Zr_2Si_2PO_{12}$ was determined by WDS and given in atomic % in Table S1. From Table S1 several

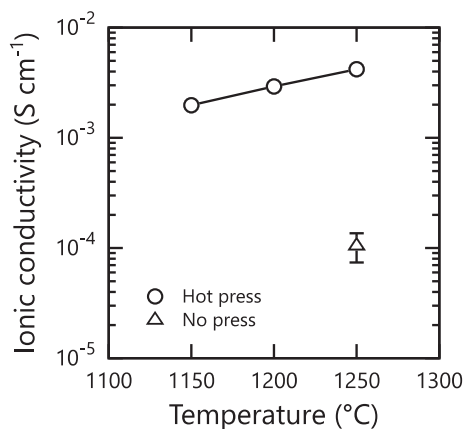**Fig. 6.** Total ionic conductivity of hot-pressed and sintered $Na_3Zr_2Si_2PO_{12}$ at room temperature.

important points are noted. Firstly, the composition of the Nasicon phase does not vary with hot-pressing temperature. Secondly, the composition of the glassy phase material is much different than that of Nasicon. It can be seen that in the glassy phase there is large decrease in the amount of Zr (78%), large increase in P (70%), moderate increase in Si (21%) and slight decrease in Na (13%) compared to the Nasicon phase. These results can be compared to chemical analysis by EDS in the literature of the glass phase in Nasicon. The EDS analysis revealed the general trend (as stated in the experimental section an accurate composition cannot be determined using EDS because of the overlap of the ZrLα and PKα X-ray lines, thus only a trend can be observed) that the glassy phase in sintered Nasicon has reduced Zr and enhanced Si and P compared to the Nasicon phase [8,11,13,24]. The trend shown by the EDS results is in agreement with the WDS results in Table S1, suggesting that indeed the glassy phase in the extruded material is from Nasicon grain boundaries (Fig. 3). In contrast after sintering at 1250 °C, with no applied stress while heating, no extruded material was observed on the sample sides. This observation agrees with the suggestion shown in Fig. 1 that stress is required to displace the glass phase from grain boundaries. This suggestion has been confirmed in creep studies on ceramic materials containing a glass phase at grain boundaries. These studies revealed that the glass phase was extruded from the sample during creep, but no glass phase was observed when only heat was applied with no stress [27–29].

3.4. Total ionic conductivity at room temperature

The ionic conductivity of the hot-pressed and sintered was determined by electrochemical impedance spectroscopy. A complex impedance Nyquist plot for the 1150, 1200 and 1250 °C hot-pressed and sintered materials at room temperature is shown in Fig. S4. The impedance data is normalized with respect to sample, L, to allow for a

direct comparison of the spectra. From Fig. S4 for the hot-pressed materials only one semi-circle (associated with grain boundary resistance) and a tail (associated with blocking electrodes) at the lower frequency side is observed over the frequency range used in this study. Consequently, only the total resistance, R_{tot}, can be measured at room temperature. It is not possible to accurately separate R_{tot} into both the R_{bulk}, bulk resistance, and R_{GB}, grain boundary resistance, contributions. In addition, for the sintered material it was not possible to accurately separate R_{tot} into R_{bulk} and R_{GB}. R_{tot} for all materials was determined from the low frequency blocking tail in the impedance spectrum by extending a straight line (shown on the figure) to the real axis (Z'). The total ionic conductivity determined from R_{tot} and sample dimensions for the 1150, 1200 and 1250 °C hot-pressed materials is shown in Fig. 6. Fig. 6 is a plot of total conductivity at room temperature versus hot-pressing temperature. The error bars for the hot-pressed materials are so small they are hidden by the symbols on the figure. Also included in Fig. 6 is the total ionic conductivity of the 1250 °C sintered material. From Fig. 6 several important points are noted. Firstly, it is observed that as the hot-pressing temperature increases the total conductivity increases from 2.0×10^{-3} S/cm at 1150 °C to 4.2×10^{-3} S/cm at 1250 °C. These values are in very good agreement with the results of Perthuis et al. [34], who observed a total conductivity of 3×10^{-3} S/cm for $Na_3Zr_2Si_2PO_{12}$ hot-pressed at 1250 °C and Lee et al. [35], who observed a total ionic conductivity of 1.8×10^{-3} S/cm for $Na_3Zr_2Si_2PO_{12}$ spark plasma sintered at 1200 °C. Spark plasma sintering is similar to hot-pressing except during application of the stress an electric current is also applied. Secondly, it can be seen that the total conductivity of the 1250 °C sintered material is about 1.1×10^{-4} S/cm. This conductivity value is an order of magnitude lower than that for the hot-pressed materials. In general total conductivity values for $Na_3Zr_2Si_2PO_{12}$ sintered over a similar temperature are typically $<1 \times 10^{-3}$ S/cm [23–25].

From the above, two questions need to be answered. Firstly, why does hot-pressing in general lead to higher total ionic conductivities compared to the sintered samples? Secondly, why does increasing the hot-pressing temperature lead to increased total ionic conductivity? In order to answer these questions, the total conductivity hence, R_{tot} must be separated into the R_B and R_{GB} contributions.

3.5. Bulk and grain boundary resistance

Because of the low total conductivity of the sintered sample, it was decided to focus the rest of this study on the higher conductivity hot-pressed materials. In order to determine the R_B and R_{GB} contributions at room temperature for the 1150, 1200 and 1250 °C hot-pressed materials the impedance spectra were recorded at lower temperatures, where separation of bulk (high frequency) and grain boundary (lower frequency) semi-circles in the complex impedance plot are clearly resolvable and hence the R_B and R_{GB} values can be determined. The low temperature resistance values are then extrapolated to room temperature using an Arrhenius plot [23,36]. Fig. 7 is an example of a complex impedance plot normalized for sample length for the 1150, 1200 and
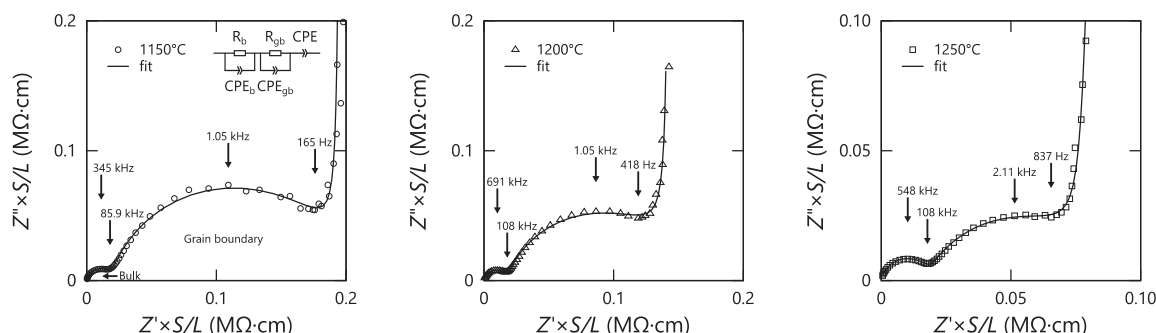

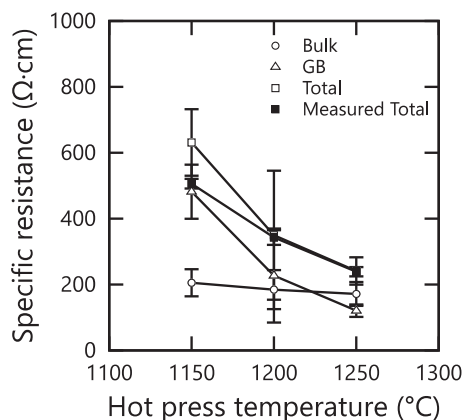**Fig. 7.** Impedance plots of hot-pressed $Na_3Zr_2Si_2PO_{12}$ at −78 °C. The equivalent circuit and fit are shown.

Fig. 8. Extrapolated and measured total specific resistance of hot-pressed $Na_3Zr_2Si_2PO_{12}$ at room temperature.

Table 3
Bulk and total conductivity of hot-pressed $Na_3Zr_2Si_2PO_{12}$ at room temperature.

Temp. (°C)	Conductivity (mS/cm)		
	Extrapolated bulk	Extrapolated total	Measured total
1150	4.9 ± 1.0	1.6 ± 0.3	2.0 ± 0.1
1200	5.9 ± 1.7	3.3 ± 1.1	2.9 ± 0.2
1250	6.0 ± 1.4	4.2 ± 0.8	4.2 ± 0.2

1250 °C hot-pressed materials tested at −78 °C. The equivalent circuit (where R and CPE indicate the resistance and constant phase element, respectively) and the fit are shown. From Fig. 7 it is observed that two semi-circles, one at high frequency and one at a lower frequency, are clearly resolvable with a semi-circle starting at the origin of the both x and y axis for the three hot-pressed materials. The capacitance values (Table S2) of the high frequency semi-circle and the lower frequency semi-circle agree with characteristic values for bulk and grain boundary, respectively. Thus, the low temperature measurement allows separation of R_{tot} into the R_B and R_{GB} contributions [23,37,38].

Arrhenius plots of logarithm TL/R, where T is temperature, versus inverse temperature for R_{tot}, R_B and R_{GB} for the 1150, 1200 and 1250 °C hot-pressed materials are shown in Fig. S5. The values for R_{tot}, R_B and R_{GB} at room temperature were obtained from these plots. Fig. 8 is a plot of extrapolated values of R_{tot}, R_B and R_{GB} from Fig. S5 at room temperature versus hot-pressing temperature. Also included in the plot is the value of R_{tot} determined from Fig. S4. Table 3 is the bulk and total conductivities determined using data from Fig. 8, Fig. 6, and sample dimensions. From Fig. 8 and Table 3 several important points are noted. Firstly, R_B is almost constant with hot-pressing temperature. There is a slight decrease from 1150 to 1200 °C. From Table 3 the bulk conductivity ranges from 5 to 6×10^{-3} S/cm. The estimated bulk conductivity of the sintered material (~4×10^{-3} S/cm) is in close agreement with the values for the hot-pressed material. The bulk conductivity for the 1200 and 1250 °C hot-pressed materials are in excellent agreement. The bulk conductivity of the 1150 °C hot-pressed materials is slightly lower than the other two. It is expected since, the composition of the Nasicon phase is the same for all three hot-pressed $Na_3Zr_2Si_2PO_{12}$ materials (Table S1) that the bulk conductivity should be the same for all three materials. One possible reason for this slight difference could be that at higher temperatures the Nasicon phase becomes more crystalline leading to higher bulk conductivity. Examination of X-ray diffraction data revealed that the crystallinity was the same at all temperatures. Another possible difference could be a result of the difference in the fraction of the monoclinic phase (Table 1). From Table 1 it is observed that at 1250 °C there is 5% less monoclinic phase compared to 1150 °C. It is known that

Table 4
Activation energy for R_{total}, R_{GB} and R_{bulk} of hot-pressed $Na_3Zr_2Si_2PO_{12}$.

Temp. (°C)	Activation energy (eV)		
	Bulk	GB	Total
1150	0.25	0.32	0.31
1200	0.25	0.32	0.31
1250	0.24	0.32	0.30

the monoclinic phase has lower bulk conductivity [39] thus, it is possible that this difference could explain the higher bulk conductivity of the material hot-pressed at 1250 °C. Secondly, there is good agreement between the measured values of R_{tot} (Fig. S4) [solid squares] and the extrapolated values (Fig. S5) [open squares]. In fact, the measured and extrapolated values of R_{tot} overlap for the 1200 and 1250 °C hot-pressed materials. This good agreement suggests that our extrapolated resistance values are accurate. As a consequence, the extrapolated total conductivity values at room temperature (Table 3) are in very good agreement with total conductivity values measured (Fig. 6) at room temperature. Thirdly, R_{GB} decreases with increasing hot-pressing temperature. This is in contrast to sintering studies, which suggested R_{GB} increases with sintering temperature > 1200 °C [15,18,20,22]. At 1250 °C R_{GB} is slightly below R_B. As a result, the total conductivity value of 4.2×10^{-3} S/cm for the 1250 °C hot-pressed material is close to bulk conductivity values (5–6 $\times 10^{-3}$ S/cm). This result is in agreement with results of M. Bayard et al. [21] and the recent work of S. Lunghammer et al. [40] and Q. Ma et al. [23] who also separated R_{tot} into R_{GB} and R_B for $Na_3Zr_2Si_2PO_{12}$ at room temperature and observed that the total conductivity was almost equal to the bulk conductivity.

3.6. Grain boundary resistance and microstructure

From Fig. 8 the results reveal that R_{tot} and hence, the total conductivity of the Nasicon materials is controlled by R_{GB}. Further proof that R_{tot} is controlled by R_{GB} is made through a comparison of the activation energy for bulk, grain boundary and total resistance for the 1150, 1200 and 1250 °C hot-pressed $Na_3Zr_2Si_2PO_{12}$ materials. The activation energy for bulk, grain boundary and total resistance was determined from the slope of the curves shown in Fig. S5 and is listed in Table 4. From Table 4 several important points are noted. Firstly, the activation energy values do not change with hot-pressing temperature. This suggests that the same mechanism is controlling at each hot-pressing temperature. This is expected for the bulk resistance since, the Nasicon composition does not change with hot-pressing temperature (Table S1). Secondly, the higher values of the activation energy for grain boundary resistance compared to those for bulk and the similarity of these values with values of the activation energy for total resistance confirm the suggestion based on Fig. 8, that total resistance and hence, total conductivity is controlled by the grain boundary resistance. Now that it is shown that R_{GB} controls total conductivity, it is of interest to show which microstructural variables(s) control R_{GB}.

From Table 2 it is observed that the porosity and grain size does not vary as the hot-pressing temperature is changed. The only microstructural variables that vary as the hot-pressing temperature is changed are the amount of ZrO_2 and the glassy phase. It has been suggested that during high temperature sintering the Nasicon phase decomposes and/or the volatilization of Na and P results in the formation of ZrO_2 particles and a glassy phase located along the grain boundaries [8,9,11,14–16,18,22,24,35]. It is known that the glassy phase has higher resistance than the Nasicon phase thus, acting as barrier to Na-ion transport [8,9,11,14,15,18,24,35]. The ZrO_2 phase will undergo a significant volume change on cooling between 1000 and 1200 °C (below the sintering temperature) as a result of a tetragonal to monoclinic phase transformation [41]. If the ZrO_2 particle size is large enough this volume change causes mechanical stresses to be generated at the ZrO_2/Nasicon interface leading to microcracking [16]. These microcracks can open

grain boundaries leading to a reduction in grain boundary conductivity. Thus, it is expected that as the amount of ZrO_2 and glassy phase increases R_{GB} should increase. From Tables 1 and 2 and Fig. 8 it is observed that as the amount of ZrO_2 increases R_{GB} decreases. Thus, it appears R_{GB} is not controlled by the ZrO_2 phase. From Table 2 and Fig. 8 it is observed that as the amount of the glassy phase decreases R_{GB} decreases. Thus, it is most likely that R_{GB} and hence, R_{tot} is controlled by the glassy grain boundary phase, in agreement with suggestions in the literature [8,9,11,14–16,18,24,35].

Now we have determined the microstructural variable (glassy phase) that controls the grain boundary resistance of the Nasicon materials we can answer the following questions: Firstly, why does hot-pressing in general lead to higher total ionic conductivities compared to the sintered samples. Secondly, why does increasing the hot-pressing temperature lead to increased total ionic conductivity.

3.7. Why does hot-pressing lead to higher total ionic conductivities compared to sintering

From Fig. 6 and Table 3 it is seen that hot-pressed $Na_3Zr_2Si_2PO_{12}$ can have total conductivities as high as 4.2×10^{-3} S/cm, approaching bulk conductivity ($5–6 \times 10^{-3}$ S/cm) whereas sintered samples of $Na_3Zr_2Si_2PO_{12}$ typically have values $<1 \times 10^{-3}$ S/cm. Since, the composition is the same, the bulk conductivity should also be the same and hence, R_B should be the same. Therefore, the difference in total conductivity must be a result of the variation in R_{GB}. It is known that for sintered Nasicon R_{GB} decreases as the sintering temperature is increased. This is a result of an increase in relative density and grain size leading to higher total conductivity. However, as the sintering temperature is further increased (>1200 °C) the amount of high resistance glassy phase along grain boundaries increases leading to an increased value of R_{GB} and hence, a decrease in total conductivity [8,9,11,14,15,18,24,35]. For example, Tiwari et al. [19] for $Na_3Zr_2Si_2PO_{12}$ sintered at 1250 °C observed a bulk conductivity of around 4.1×10^{-3} S/cm, similar to bulk values observed in this study, yet their total conductivity was only around 3.1×10^{-4} S/cm ($\sim$ order of magnitude lower than that exhibited by the results in the current study) as a result of high grain boundary resistance. In contrast as seen in Table 3 for hot-pressed $Na_3Zr_2Si_2PO_{12}$ it is observed that the total conductivity approaches bulk conductivity values, because of reduced grain boundary resistance (Fig. 8). The reason for the difference is the application of the applied stress. The presence of an applied stress during hot-pressing promotes the flow of the glass phase from the sample interior towards the exterior, thus reducing the amount of the glassy phase along grain boundaries. This result is shown in Table 2 where it can be seen that at 1250 °C the hot-pressed sample contained about 5 area % glass phase, whereas the sintered sample contained about double this amount, about 10 area % glass phase. Furthermore, as stated earlier no glass was observed on the surfaces of the sintered sample whereas as shown in Fig. 5 an extruded glass phase is observed after hot-pressing. The reduction of the glass phase along Nasicon grain boundaries leads to a lower R_{GB} and hence, a higher total conductivity compared to conventional sintering where no stress is applied (Fig. 1).

The flow of glassy grain boundary phase to the outside surfaces under the hot-pressing stress agrees with several creep studies of ceramic materials containing a glassy grain boundary phase. Clarke [28] observed an extruded glass phase on sample surfaces of an alumina glass composite after creep, whereas no extruded material was observed on a sample only heated with no stress. Besson et al. [27] observed on creep studies of a nitrogen ceramic containing a glassy phase that the presence of an applied stress caused a marked decrease in the amount of the glass phase along grain boundaries in the interior of the sample compared to the exterior. No change in the amount of glass phase was observed in samples only heated with no applied stress. Badwal et al. [29] observed for the case of polycrystalline ZrO_2 containing a silicon-based glass phase along the ZrO_2 grain boundaries during creep that as the temperature was increased at fixed stress R_{GB} decreased while R_B remained

constant, similar to the results of this study. They also observed that as the stress was varied from 10 to 100 MPa at 1200 °C that the grain-boundary resistance decreased dramatically whereas increasing the stress had no effect on lattice resistance. Transmission electron microscopy studies showed that grain boundary glass phase relocating from boundaries perpendicular to those parallel to the stress. It was suggested that the relocation of the low conductivity glass phase enhanced contact between grains leading to a decreased value of R_{GB} [29]. Consequently, it is believed, that the higher conductivity of the hot-pressed material $Na_3Zr_2Si_2PO_{12}$ compared to the sintered $Na_3Zr_2Si_2PO_{12}$ is a result of the applied stress during hot-pressing which reduces the amount of the high resistance glassy phase along grain boundaries leading to a lowering of R_{GB} and hence, a higher total conductivity.

3.8. Why does increasing the hot-pressing temperature lead to increased total ionic conductivity

From Fig. 6 and Table 3 it is observed that as hot-pressing temperature increases the total conductivity increases. From Fig. 8 this behavior is related to a decrease in R_{GB} with increasing temperature. There are possible reasons that can influence how R_{GB} changes with temperature. As discussed earlier these are related to the change in the amount of the glassy phase along the Nasicon grain boundaries. One possible reason is that as the temperature is increased, the viscosity of the glassy phase will decrease leading to a higher flow rate under stress [27–29]. This decrease in viscosity could be a result of not only increasing temperature but also due to a change in glass composition as temperature is increased. The fact that the activation energy for grain boundary resistance is constant at the different hot-pressing temperatures (Table 4) would suggest that the composition of the glass does not change with hot-pressing temperature. In addition, it has been shown for the case of von Alpen Nasicon, $Na_{3.1}Zr_{1.55}Si_{2.3}P_{0.7}O_{11}$ hot-pressed at 1025 to 1100 °C, it was observed that the composition of the glass phase did not change with hot-pressing temperature [42]. Furthermore, since the grain size of the three hot-pressed materials is similar (Table 2) it is most likely that the change in R_{GB} with increasing the hot-pressing temperature is a result of a reduced thickness of the glassy boundary phase. As a first attempt the brick-layer model was selected to calculate the glass phase thickness.

In many polycrystalline solid electrolytes, the microstructure can be approximated by a brick layer model of cubic grains separated by more resistive thin homogenous grain boundary layers [43–49]. Using the brick layer model with capacitance data from the impedance spectra and a knowledge of the grain size an estimate of the grain boundary thickness can be made. In this model R_{GB} varies directly with grain boundary thickness [43]. Thus, reducing grain boundary thickness leads to a reduced value of R_{GB}. For $Na_3Zr_2Si_2PO_{12}$ it is assumed that the Nasicon grains are surrounded by a glassy boundary phase of thickness, δ_{GB}. Using the brick layer model and data from the impedance spectra and the grain size an estimate of the glassy boundary phase thickness as a function of hot-pressing temperature was attempted using the equation below [43–49].

$$\delta_{GB} = d_{bulk} \frac{C_{bulk} \bullet \varepsilon'_{GB}}{C_{GB} \bullet \varepsilon'_{bulk}} \qquad (4)$$

Where C_{bulk} is the bulk capacitance at the apex of bulk semi-circle, C_{GB} is the grain boundary capacitance at the apex of grain boundary semi-circle, d_{bulk} is the grain size and ε_{bulk} is the permittivity of the bulk and ε_{GB} is the permittivity of the grain boundary. For a first approximation assume [44,48,49].

$$\varepsilon'_{GB} = \varepsilon'_{bulk} \qquad (5)$$

In which case Eq. (1) becomes:

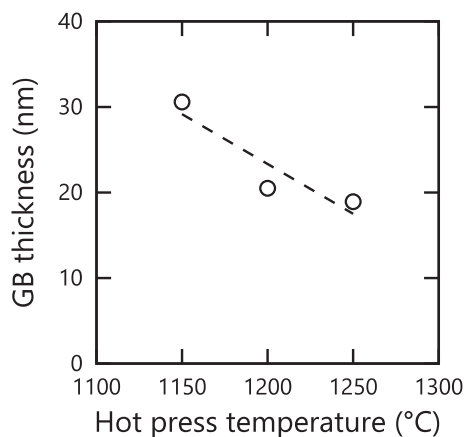$$\delta_{GB} = d_{bulk} \frac{C_{bulk}}{C_{GB}} \qquad (6)$$

Fig. 9. Glass thickness as a function of hot-pressing temperature.

C_{bulk} and C_{GB} were determined at the maximum of each semi-circle, where $RCf_{max} = 1$, (f_{max} is the frequency), from the impedance plot for the 1150, 1200 and 1250 °C hot-pressed materials at −78 °C (Fig. 7) and are listed in Table S2. The grain size is listed in Table 2. Using this data, a plot of glass thickness versus hot-pressing temperature was constructed and is shown in Fig. 9. A least squares fit is shown. It should be noted that the model predicts a grain boundary glass thickness in the nm range. These values are smaller than those observed in Fig. 3. A similar observation has been observed for the case of 3Y-TZP materials containing an intergranular glass phase [50]. High resolution transmission electron microscopy was conducted on the 3Y-TZP materials in order to confirm that the thickness of the intergranular glass was in the nm range. High resolution transmission electron microscopy is required and underway to confirm the results of Fig. 9. From Fig. 9 there is a general trend in that glass thickness decreases with increasing hot-pressing temperature. As the hot-pressing temperature is increased a reduction in the viscosity of the glass occurs leading to a reduction in glass thickness, which leads to a decreased value of R_{GB} and hence, a higher total conductivity. This suggestion agrees with the results in Fig. 6 and Table 3, which reveal that as the hot-pressing temperature increases total conductivity increases.

It should be noted that in many instances the assumption of $\varepsilon_{GB} = \varepsilon_{bulk}$ is not valid [43,51]. Even if the assumption of $\varepsilon_{GB} = \varepsilon_{bulk}$ is not valid, this will not change the qualitative trend shown in Fig. 9. It only changes the magnitude of the glass thickness.

4. Conclusions

Hot-pressing $Na_3Zr_2Si_2PO_{12}$ at 1250 °C achieved a total conductivity of 4.2×10^{-3} S/cm at room temperature, approaching bulk conductivity values ($5–6 \times 10^{-3}$ S/cm), whereas sintered samples of $Na_3Zr_2Si_2PO_{12}$ typically have values $<1 \times 10^{-3}$ S/cm. The higher total conductivity of the hot-pressed material is a result of an applied stress during hot-pressing. The applied stress at high temperatures causes a reduction in the thickness of the high resistance glassy phase along Nasicon grain boundaries leading to a lower grain boundary resistance and hence, a higher total conductivity than that observed for sintered samples where no applied stress is used. Hot-pressing of polycrystalline solid electrolytes containing a glassy grain boundary phase can be used to reduce grain boundary resistance compared to conventional sintering, resulting in high total ionic conductivities with values approaching bulk conductivity values.

CRediT authorship contribution statement

Makoto Kimura: Writing – original draft, Investigation, Formal analysis. **Kang-Ting Tseng:** Investigation, Data curation. **Jeff**

Wolfenstine: Writing – original draft, Conceptualization. **Jeff Sakamoto:** Writing – review & editing, Supervision, Conceptualization.

Declaration of competing interest

There are no conflicts of interest to declare.

Data availability

Data will be made available on request.

Appendix A. Supplementary data

Supplementary data to this article can be found online at https://doi.org/10.1016/j.ssi.2024.116561.

References

[1] Q. Ma, F. Tietz, ChemElectroChem 7 (2020) 2693–2713.
[2] Y. Kim, H. Kim, S. Park, I. Seo, Y. Kim, Electrochem. Acta 191 (2016) 1–7.
[3] J. Kim, H.J. Seung, S. Bhavaraju, A. Eccleston, S.O. Kang, J. Electroanal. Chem. 759 (2015) 201–206.
[4] S. Modak, J. Valle, K.T. Tseng, J. Sakamoto, D.G. Kwabi, ACS Appl. Mater. Interfaces 14 (2022) 19332–19341.
[5] J.B. Goodenough, Proc. Soc. Lond. A 393 (1984) 215–234.
[6] J.B. Goodenough, H.P. Hong, J.A. Kafalas, Mater. Res. Bull. 11 (1976) 203–220.
[7] F. Krok, Solid State Ionics 24 (1987) 21–28.
[8] S. Naqash, F. Tietz, E. Yashenskikh, M. Muller, O. Guillon, Solid State Ionics 336 (2019) 57–66.
[9] S. Naqash, D. Sebold, E. Tietz, O. Guillon, J. Am. Ceram. Soc. 102 (2019) 1057–1070.
[10] A.K. Kuriakose, T.A. Wheat, A. Ahmad, J. DiRocco, J. Am. Ceram. Soc. 67 (1984) 179–183.
[11] A. Ahmad, T.A. Wheat, K. Kuriakose, J.D. Canaday, A.G. McDonald, Solid State Ionics 24 (1987) 89–97.
[12] R.S. Gordon, G.R. Miller, B.J. McEntire, E.D. Beck, J.R. Rasmussen, Solid State Ionics 3 (4) (1981) 243–248.
[13] I.K. Lloyd, T.K. Gupta, B.O. Hall, Solid State Ionics 11 (1983) 39–44.
[14] A. Hooper, J. Electroanal. Chem. 109 (1980) 161–166.
[15] R.O. Fuentes, F. Figueiredo, F.M.B. Marques, J.L. Franco, Ionics 8 (2002) 383–390.
[16] W. Go, J. Kim, J. Pyo, J.B. Wolfenstine, Y. Kim, ACS Appl. Mater. Interfaces 13 (2021) 52727–52735.
[17] O. Bohnke, S. Ronchetti, D. Mazza, Solid State Ionics 122 (1999) 127–136.
[18] O. Fuentes, F. Figueiredo, F.M.B. Marques, J.L. Franco, Solid State Ionics 140 (2001) 173–179.
[19] A. Tiwari, D. Meghnani, R. Mishra, R.K. Tiwari, A. Patel, R.K. Singh, J. Power Sources 580 (2023) 233365.
[20] C. Wen, Z. Luo, H. Liang, X. Liu, W. Lei, A. Lu, Appl. Phys. A Mater. Sci. Process. 128 (2022) 71–83.
[21] M.L. Bayard, G.G. Barna, J. Electroanal. Chem. 91 (1978) 201–209.
[22] S. Liu, C. Zhou, Y. Wang, W. Wang, Y. Pei, J. Kieffer, R.M. Lane, ACS Appl. Mater. Interfaces 12 (2020) 3502–3509.
[23] Q. Ma, C.H. Tasi, X.K. Wei, M. Heggen, F. Tietz, J.T.S. Irvine, J. Mater. Chem. A 7 (2019) 7766–7776.
[24] H.B. Kang, N.H. Cho, J. Mater. Sci. 34 (1999) 5005–5013.
[25] M. Guin, F. Tietz, J. Power Sources 273 (2015) 1056–1064.
[26] J.W. Fergus, Solid State Ionics 227 (2012) 102–112.
[27] J.E. Besson, S. Streicher, T. Chartier, P. Goursat, J. Mater. Sci. Lett. 5 (1986) 803–805.
[28] D.R. Clarke, J. Mater. Sci. 20 (1985) 1321–1332.
[29] S.P.S. Badwal, F. Ciacchi, M.V. Swain, V. Zelizko, J. Am. Ceram. Soc. 73 (1990) 2505–2507.
[30] F. Izumi, K. Momma, Solid State Phenom. 130 (2007) 15–20.
[31] Japanese Industrial Standards JIS, G 0551, Steels-Micrographic Determination of the Apparent Grain Size, 2020.
[32] D.W. Lee, C.M. Jensen, J. Chem. Educ. 77 (2000) 629.
[33] S.J.B. Reed, Electron Probe Microanalysis, 2nd ed., Cambridge University Press, 1993.
[34] H. Perthuis, Ph. Colomban, Mater. Res. Bull. 19 (1984) 621–631.

[35] J.S. Lee, C.M. Chang, Y.I. Lee, J.H. Lee, S.H. Hong, J. Am. Ceram. Soc. 87 (2004) 305–307.
[36] E. Lilley, J.E. Strutt, Phys. Status Solidi 54 (1979) 639–650.
[37] R.A. Huggins, Ionics 8 (2002) 300–313.
[38] J.T.S. Irvine, D.C. Sinclair, A.R. West, Adv. Mater. 2 (1990) 132–138.
[39] L. Ran, A. Baktash, M. Li, Y. Yi, B. Demir, T. Lin, M. Li, M. Rana, I. Gentle, L. Wang, D.J. Searles, R. Knibbe, Energy Storage Mater. 40 (2021) 282–291.
[40] S. Lunghammer, Q. Ma, D. Rettenwander, I. Hanzu, F. Tietz, H.M.R. Wilkening, Chem. Phys. Lett. 701 (2018) 147–150.
[41] D.J. Green, J. Mater. Sci. 20 (1985) 2639–2646.
[42] T.-K. Tseng, Unpublished Work, 2024.
[43] T. Van Dijk, A.J. Burggraff, Phys. Status Solidi 63 (1981) 229–240.

[44] S.M. Haile, D.L. West, J. Campbell, J. Mater. Res. 13 (1998) 1576–1595.
[45] A.I. Ioffe, M.V. Inozemtsev, A.S. Lipilin, M.V. Perfilev, S.V. Karpachov, Phys. Status Solidi 30 (1975) 87–94.
[46] M.J. Verkerk, B.J. Middelhuis, A.J. Burggraff, Solid State Ionics 6 (1982) 159–170.
[47] J. Fleig, J. Maier, J. Eur. Ceram. Soc. 19 (1999) 693–696.
[48] M.C. Martin, M.L. Mecartney, Solid State Ionics 161 (2003) 67–79.
[49] W.E. Tenhaeff, E. Rangasamy, Y. Wang, A. Sokolov, J. Wolfenstine, J. Sakamoto, N. J. Dudney, ChemElectroChem 2 (2014) 375–378.
[50] M. Godickemeier, B. Michel, A. Orliukas, P. Bohac, K. Saski, L. Gauckler, H. Heinrich, P. Schwander, G. Kostorz, H. Hofmann, O. Frei, J. Mater. Res. 9 (1994) 1228–1240.
[51] G.M. Christie, F.P.F. van Berkel, Solid State Ionics 83 (1996) 17–27.